Tetrahedron 69 (2013) 2720–2732

Contents lists available at SciVerse ScienceDirect

Tetrahedron

journal homepage: www.elsevier.com/locate/tet

Bromine-substituted *p*-nitrostilbene derivatives: synthesis, crystal structural studies, photoluminescence and the heavy atom effect on the singlet oxygen generation by two-photon absorption

Fang Gao [a,*], Xinchao Wang [a], Suna Wang [b], Meng Liu [a], Xiaojiao Liu [a], Xiaojuan Ye [a], Hongru Li [a,*]

[a] School of Chemistry and Chemical Engineering, Chongqing University, Chongqing 400044, China
[b] School of Chemistry and Chemical Engineering, Liaocheng University, Liaocheng 252059, China

ARTICLE INFO

Article history:
Received 7 November 2012
Received in revised form 22 January 2013
Accepted 1 February 2013
Available online 8 February 2013

Keywords:
Two-photon absorption
Crystal structure
Photoluminescence
Singlet oxygen
Near-IR laser

ABSTRACT

A variety of linear and side-chained *p*-nitrostilbene derivatives with various numbers of bromine atoms were prepared to survey the crystal structural properties, the photoluminescence, and heavy atom effect on the singlet oxygen generation by two-photo absorption (TPA). Single crystals of 4-nitro-4′-(4″-bromo-phenyl-methyl-oxy)-diphenylethylene (**C2**), 4-nitro-4′-(3″,5″-dibromo-phenyl-methyl-oxy)-diphenyl-ethylene (**C3**), 4-nitro-4′-(2′,3″,4′,5″,6″-pentabromo-phenyl-methyl-oxy)-diphenylethylene (**C4**) were obtained, and the structural characteristics were analyzed by X-ray diffraction. One- and two-photon optical properties of the photosensitizers are shown dependence on the numbers of substituted bromine atoms. While TPA cross-sections of the photosensitizers are diminished more considerably, singlet oxygen quantum yields of the photosensitizers are enhanced at some extents by the substituted bromine atoms. Side-chained photosensitizers display correspondingly higher singlet oxygen quantum yields and larger TPA cross-sections than the molecules with single bromine-substituted aromatic segment. Molecular modeling was also performed to reveal the fundamental reasons of the experimental observation. Photooxidation reaction of singlet oxygen with some substrates was employed to confirm singlet oxygen generation under one- and two-photon irradiation.

© 2013 Published by Elsevier Ltd.

1. Introduction

Chemistry and biochemistry of singlet oxygen ($^1O_2$) have been drawing considerable attention since its discovery in the 1960s. An electronically excited molecule of oxygen ($^1O_2$) is produced normally through photoinduced energy transfer between the triplet-sensitizing molecule absorbing incident near ultraviolet or visible light irradiation and the ground state oxygen.[1] Singlet oxygen exhibits distinguished reactivity with a wide variety of electron-rich molecules, which has been found in many synthetic fields.[2–6] Of particular interest for scientists is that singlet oxygen plays significant photodynamic therapy (PDT) role due to its efficiently treating tumor cells.[7–12] In recent years, the utilization of available near-IR laser to generate singlet oxygen becomes one of the hot topics as near-IR light has several unique advantages such as low energy, deep penetration, and negligible damage to the normal biological tissues. TPA dyes open up the future of near-IR PDT application.[13–15] However, near-IR TPA photodynamic therapy is limited because of the absence of TPA photosensitizers with ideal properties such as high singlet oxygen quantum yields, large TPA cross-sections, and excellent biological compatibility. A number of chemical approaches have been tried to obtain TPA singlet oxygen photosensitizers.[15–23] For example, dimer or trimer porphyrins were demonstrated with large TPA cross-sections.[16–18] Heavy atom effect is regarded as an efficient strategy to improve the quantum yield of single oxygen of photosensitizers under two-photon irradiation.[19] It has been reported that non-linear optical properties of the organic molecules exhibited certain dependence on heavy atom effect.[24] However, it is some surprised that the effects of the numbers of substituted bromine atoms on TPA generation of singlet oxygen by the photosensitizers have been reported seldomly so far. It is necessary to optimize the numbers of substituted bromine atoms for a new TPA singlet oxygen photosensitizer.

The introduction of side chain could improve the density of some functional segments in a molecule. *p*-Nitrostilbene can be utilized as parent segment to construct TPA singlet oxygen photosensitizers due to its remarkable TPA nature. In this study, a variety of *p*-nitrostilbene derivatives bearing with various numbers of substituted bromine atoms were synthesized. As shown in Scheme 1, the

* Corresponding authors. E-mail address: fanggao1971@gmail.com (F. Gao).

0040-4020/$ – see front matter © 2013 Published by Elsevier Ltd.
http://dx.doi.org/10.1016/j.tet.2013.02.010

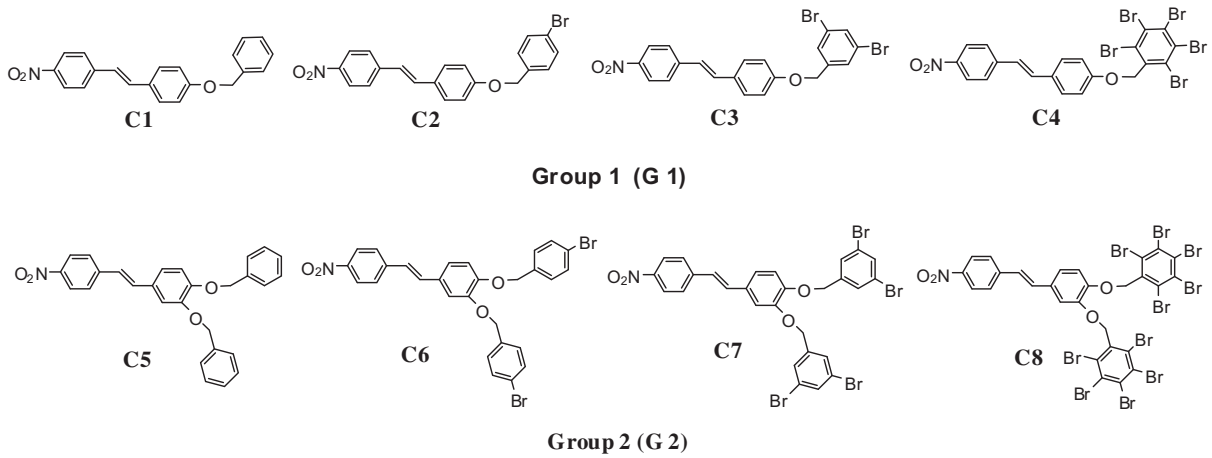

Scheme 1. Chemical structures of the photosensitizers studied in this article.

numbers of bromine atoms in the side-chained photosensitizers (Group 2, **C5**–**C8**) are correspondingly twice as many as those in the linear ones (Group 1, **C1**–**C4**). It is assumed that heavy atom effect on one- and two-photon optical properties could be more remarkable if TPA photosensitizers contain more bromine atoms, which are considered to be favorable for intersystem crossing of the excited states. Consequently, it can be assumed that one- and two-photon fluorescence emission could be reduced by the substituted bromine atoms, and the quantum yields of singlet oxygen could be improved. Furthermore, the effects of the substituted bromine atoms on TPA cross-sections of the photosensitizers could be revealed. This study may provide chemical insight to design and synthesis TPA singlet oxygen photosensitizers. In this work, we performed cooperative experimental and molecular modeling to reveal the interrelationship between the numbers of substituted bromine atoms and the structural characteristics and one- and two-photon optical properties of the photosensitizers.

Singlet oxygen generation by near-IR TPA photosensitizers is commonly detected by the determination of characteristics phosphorescence photoluminescence (1270 nm). This study utilized the chemical reaction of singlet oxygen with some substrates to produce photooxidation products, which in turn confirm the generation of singlet oxygen by these photosensitizers under near-IR femtosecond laser irradiation.

2. Results and discussion

2.1. X-ray crystallography

Although some crystallographic disorder was formed in single crystals of **C2** and **C4** (Fig. 1a and c), for example, two oxygen atoms occupied two positions (O(3), and O(3)′) with half rate in the single crystal of **C4**, the correct molecular structures of **C2**, **C3**, and **C4** could be analyzed (Fig. 1, also see Supplementary data). Fig. 1 also suggests that the two adjacent benzene rings in diphenylethylene parts of **C2**, **C3**, and **C4** tend to be coplanar, and the dihedral angles between them in **C2**, **C3**, and **C4** are 22.93°, 9.44°, and 10.45°. The bromine-containing-phenyl rings are deviated considerably from the adjacent benzene rings (connecting via ether bond) in the diphenylethylene parts of **C2**, **C3**, and **C4** (Fig. 1), and the dihedral angles between them are increased by the substituted bromine atoms (67.33°, 73.53°, and 83.82° for **C2**, **C3**, and **C4**). The results reflect the effect of heavy weight bromine atoms on the crystal geometry of **C2**, **C3**, and **C4**. Fig. 2 shows that there is CH···π (namely σ–π) stacking intermolecular interaction in the crystals of **C2**, **C3**, and **C4** (**C3**, symmetry codes: A: $-x$, $-y$, $1-z$; B: $1-x$, $1-y$, $1-z$; **C4**, symmetry codes: A: x, $0.5-y$, $0.5+z$; B: x, $0.5-y$, $-0.5+z$), which could be the major factor dominating the growth and stabilizations of the crystals. The analysis shows that the distance of C–H···π is 2.810(2) Å in the crystal of **C2**, 3.220(3) Å in the crystal of **C3**, and 2.946(2) Å in the crystal of **C4**. We further observed intermolecular π···π stacking interaction between nitro-phenyl rings in the single crystal of **C3**, and the distance between two rings centers ($d1$) was 3.982(1) Å. Similar CH···π or π···π stacking interaction has been ever observed in other Ar–O–CH_2–stilbene derivatives.[25]

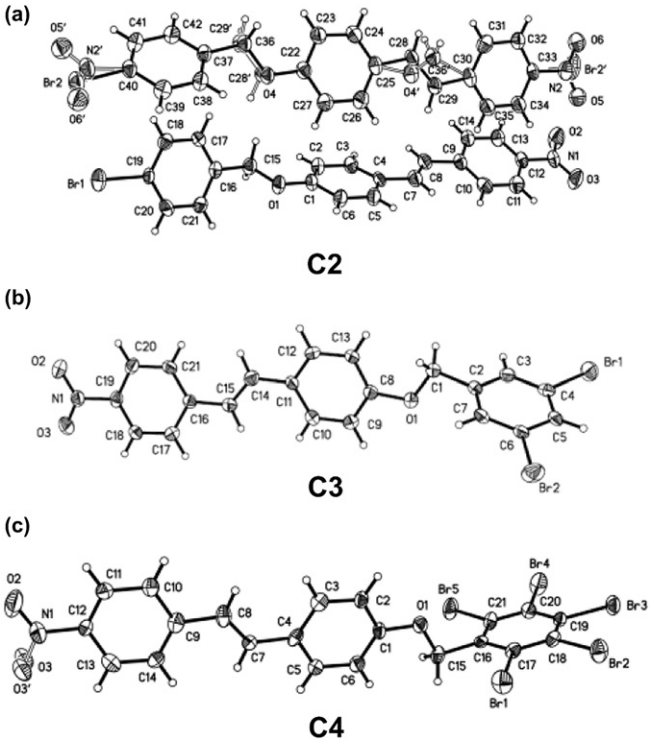

Fig. 1. ORTEP drawing of **C2**, **C3**, and **C4** with thermal ellipsoids at 50% probability.

2.2. Effects on one-photon absorption and emission spectra

One-photon absorption and emission spectra of the photosensitizers were investigated in various solvents. Representative linear absorption and emission spectra of the photosensitizers in tetrahydrofuran (THF) are available in Fig. 3. Typical one-photon

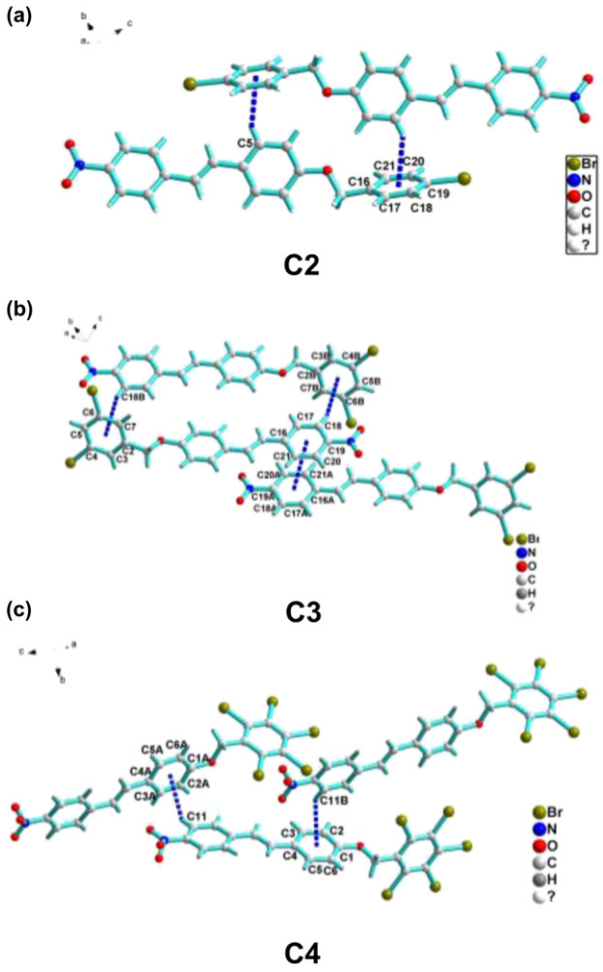

Fig. 2. View of the C–H···π and π···π stacking interactions in **C2**, **C3**, and **C4**.

absorption and emission spectral parameters of **C1**–**C8** in various solvents are given in Table 1. The absorption and emission maxima of **C1**–**C8** shift to longer wavelengths in polar solvents (such as from benzene to CH_3CN). This suggests that internal charge transfer could exist in the ground and excited states of **C1**–**C8**.[26]

The maximal absorption and emission wavelengths of **C1**–**C8** are shifted hypsochromically by the substituted bromine atoms (Fig. 3, also see Supplementary data). These could be caused by the reduced intramolecular charge transfer and lowered coplanarity of **C1**–**C8** by bromine atoms. We need mention that the number of bromine atoms in the phenyl unit could not seriously affect the donating capability of the Ph–CH_2–O– segment, because it is not a conjugated structure and there is an sp^3 –CH_2– between the phenyl unit and oxygen atom. The main reason could be due to the lowered coplanarity of **C1**–**C8** by bromine atoms, and it increases the difficulty of internal charge transfer accordingly. It is also noticed that the maximal absorption and emission wavelengths of **C5**–**C8** are red-shifted accordingly as comparison with **C1**–**C4** in various solvents (ca. 10–30 nm, Table 1, or typically shown in Fig. 4a). It is assumed that internal charge transfer of **C5**–**C8** could be improved due to more numbers of oxygen donors. This could explain the corresponding red-shift of the absorption and emission maxima of **C5**–**C8** with respect to those of **C1**–**C4**.

Seen from Table 1, the maximal molar extinction coefficients of **C5**–**C8** are correspondingly larger than those of **C1**–**C4** in modest polar solvents such as THF and EtOAc (such as **C1**: 0.146×10^5 mol^{-1} cm^{-2}; **C5**: 0.216×10^5 mol^{-1} cm^{-2}). While in non-polar solvents (such as benzene) or stronger polar solvents (such as CH_2Cl_2 and CH_3CN), the maximal molar extinction coefficients of **C5**–**C8** are accordingly similar to those of **C1**–**C4**. Although the solvent refractive index and its dispersion could be the part of reason for the above results,[27] the main reason could be due to internal charge transfer.[28] The absorption spectra determined in various solvents suggest that the maximal peaks of the photosensitizers could be from internal charge transfer.[28] In benzene, the difference on the internal charge transfer between **C5**–**C8** and **C1**–**C4** could not be obvious due to the low polarity of the solvent. Hence, the maximal molar extinction coefficients are correspondingly similar. While in very strong polar solvents such as CH_2Cl_2 or CH_3CN, internal charge transfer tends to be diminished by adiabatic molecular torsion, hence, the maximal molar extinction coefficients of **C5**–**C8** are also accordingly close to those of **C1**–**C4** as well. But in the modest polar solvents such as THF and EtOAc, the difference on the internal charge transfer between **C5**–**C8** and **C1**–**C4** could exhibit the most remarkable due to the absence of large adiabatic molecular deviation. As a consequence, the maximal molar extinction coefficients of **C5**–**C8** are correspondingly larger than those of **C1**–**C4**.

2.3. Molecular modeling

Molecular geometry optimization also suggests that the coplanarity of **C1**–**C8** are decreased by the substituted bromine atoms (typically shown in Fig. 5, also see Supplementary data). It is obvious that **C5**–**C8** exhibit more extension in the space than **C1**–**C4**. Table 2 presents representative optimized geometry parameters of the photosensitizers. The data demonstrate that the dihedral angles between the phenyl ring carrying bromine atoms and its adjacent phenyl ring connected via ether linkage bond (i.e., Ar–CH_2–O–Ph) are enhanced by the substituted bromine atoms, which is consistent with the single crystal analysis.

The oscillator strengths (f), and the composition (weightage) of the most important microstates in the anterior excited states of the photosensitizers were calculated out to analyze the relationship between the frontier orbital transition and the properties of the ground and excited states (see Supplementary data). The most important states mean that there is some transition probability (namely weightages) between the frontier orbitals.[29] It is noticed that HOMO→LUMO transition of the photosensitizers possess the largest f values for both the absorption (such as **C2**, 0.7528; **C6**, 0.7018) and the emission spectra (such as **C2**, 1.284; **C6**, 1.170) with remarkable weightages (such as for absorption: **C2**, **C6**, 99%; for emission: **C2**, **C6**, 100%). The results suggest that the absorption and emission of **C1**–**C8** are from HOMO→LUMO electron transition. Symmetric HOMO and LUMO orbitals with the electron cloud density distribution of the photosensitizers mean that the ground and excited states of the photosensitizers are characterized with (π,π) transition with internal charge transfer nature (typically shown in Fig. 6, also see Supplementary data).

The sum of charge (e) in phenyl ring containing bromine atoms tends to be more negative due to electron-withdrawing effect of bromine atoms (Table 3). More important, the coplanarity of **C1**–**C8** is seriously diminished by bromine atoms. As a consequence, the electron-donating properties of Ar–CH_2–O– part in **C1**–**C8** could be lowered by bromine substitution. It could be seen from the dipole moment differences between the ground and excited states of the photosensitizers. Table 3 also shows that the dipole moment differences of the photosensitizers are lowered by the substituted bromine atoms. The data indicate that the extent of internal charge transfer of **C1**–**C4** and **C5**–**C8** is decreased gradually by bromine atoms. **C5**–**C8** have more numbers of oxygen donors (namely Ar–CH_2–O–), hence, the electronic delocalization and corresponding properties are truly affected. The extent of internal charge transfer during HOMO→LUMO of **C5**–**C8** are correspondingly

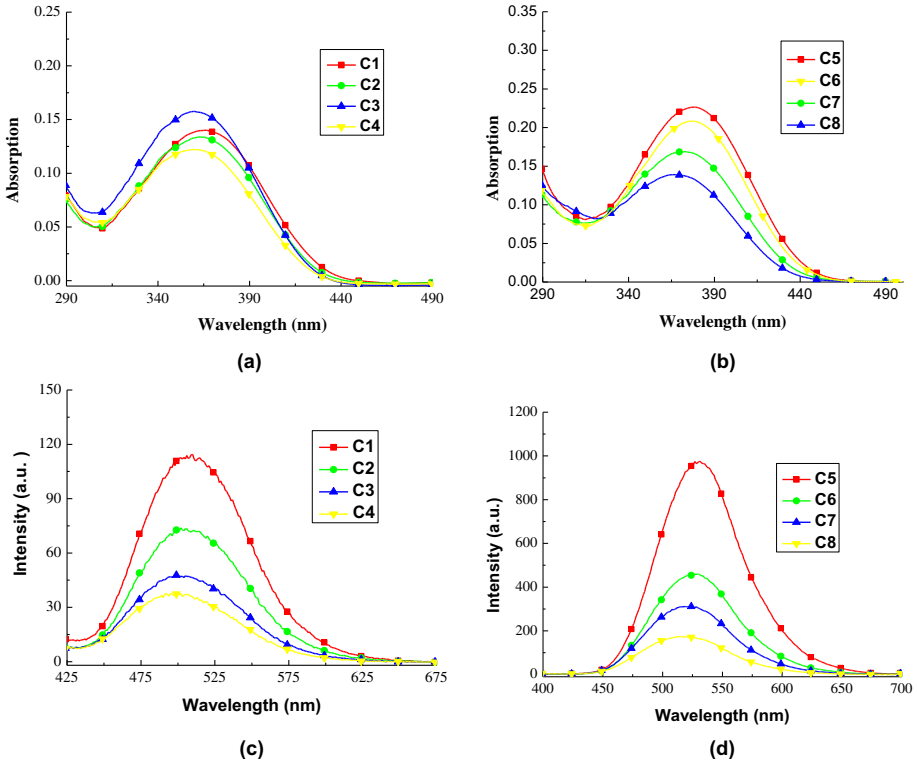

Fig. 3. Representative UV/visible absorption and emission spectra of the photosensitizers in THF (c: 1×10^{-5} mol/L) determined under the same experimental condition for absorption and emission spectra, respectively. (a) and (b): The absorption spectra; (c) and (d): the emission spectra.

Table 1
Representative one-photon spectral parameters of the photosensitizers in various solvents

Solvents		Photosensitizers							
		G1				G2			
		C1	**C2**	**C3**	**C4**	**C5**	**C6**	**C7**	**C8**
Benzene	$\lambda_{abs,max}$	360	357	356	354	373	372	369	369
	ε_{max} ($\times10^5$)	0.127	0.112	0.121	0.099	0.124	0.104	0.131	0.109
	$\lambda_{em,max}$	—	—	—	—	494	492	483	472
	Φ	Weak	Weak	Weak	Weak	0.062	0.017	0.002	0.001
EtOAc	$\lambda_{abs,max}$	362	360	358	357	375	374	369	368
	ε_{max} ($\times10^5$)	0.111	0.114	0.102	0.128	0.174	0.236	0.194	0.146
	$\lambda_{em,max}$	514	510	503	502	531	525	523	514
	Φ	0.049	0.030	0.024	0.016	0.290	0.202	0.123	0.057
THF	$\lambda_{abs,max}$	366	364	356	355	379	378	371	370
	ε_{max} ($\times10^5$)	0.146	0.136	0.159	0.125	0.216	0.208	0.172	0.139
	$\lambda_{em,max}$	513	508	506	501	531	526	523	517
	Φ	0.097	0.062	0.039	0.034	0.390	0.309	0.177	0.102
CH_2Cl_2	$\lambda_{abs,max}$	376	367	364	362	381	380	376	374
	ε_{max} ($\times10^5$)	0.200	0.355	0.272	0.289	0.221	0210	0.193	0.138
	$\lambda_{em,max}$	545	541	538	537	560	556	549	548
	Φ	0.193	0.190	0.176	0.174	0.151	0.073	0.065	0.045
CH_3CN	$\lambda_{abs,max}$	371	367	366	364	379	376	375	372
	ε_{max} ($\times10^5$)	0.273	0.242	0.249	0.161	0.276	0.247	0.163	0.106
	$\lambda_{em,max}$	562	561	554	553	—	—	—	—
	Φ	0.083	0.072	0.056	0.043	Weak	Weak	Weak	Weak

$\lambda_{abs,max}$: nm, the maximal absorption wavelength; ε, mol^{-1} cm^{-2}, the maximal molar extinction coefficient; $\lambda_{em,max}$: nm, the maximal emission wavelength. Φ: the fluorescence quantum yield.

larger than those of **C1**–**C4** due to containing more oxygen donors. Hence, **C5**–**C8** show accordingly more dipole moment differences between the ground and excited states than **C1**–**C4** (Table 3).

It is assumed that the values of absorption maxima could be from the vertical transition from S_0 states to the Franck–Condon S_1 states, and the numbers of the normal emission maxima may be identical to the decay of S_1 states to the corresponding Franck–Condon S_0.[30] Hence, the calculated absorption and emission maxima of the photosensitizers are considered to be equal to the corresponding frontier orbital transition energy differences, which represent as singlet–singlet transition energies. HOMO–LUMO energy gaps (E: eV) of **C1**–**C4** and **C5**–**C8** in the ground and excited states are improved by the bromine substitution (Table 4), which could interpret that the maximal absorption and emission wavelengths of **C1**–**C8** are blue-shifted by bromine substitution. Table 4 further shows that **C5**–**C8** have correspondingly less HOMO–LUMO gaps in the ground and excited states than **C1**–**C4**. These are further evidences that the maximal absorption and emission wavelengths of

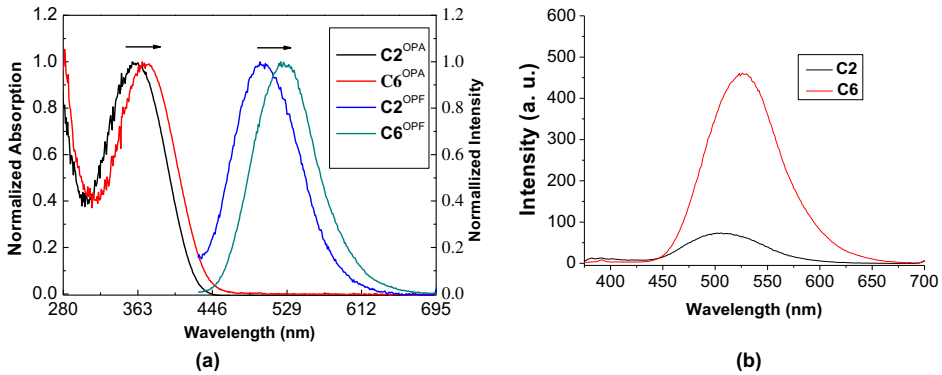

Fig. 4. Typical comparisons one-photon absorption and emission spectra of **C2** and **C6** in THF. (a): Normalized linear absorption and emission spectra of **C2** and **C6** in THF; (b): actual one-photon emission spectra of **C2** and **C6** in THF, performed at the same experimental condition.

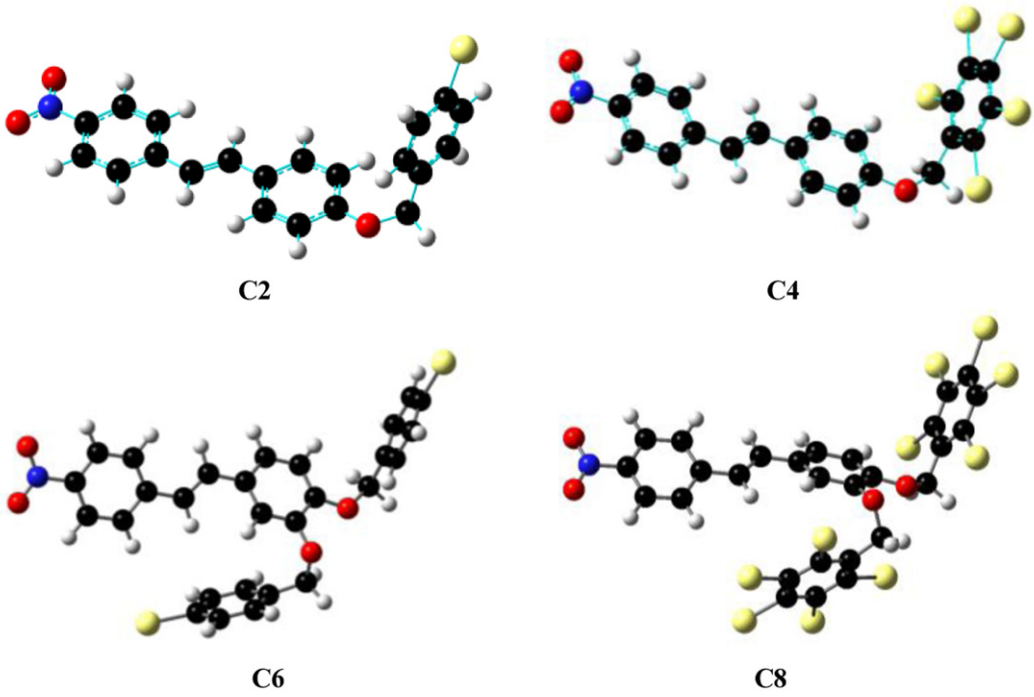

Fig. 5. Typical comparisons of the theoretically optimized geometry of **C2**, **C4**, **C6**, and **C8**.

Table 2
Theoretically optimized geometry parameters of **C1**–**C8**

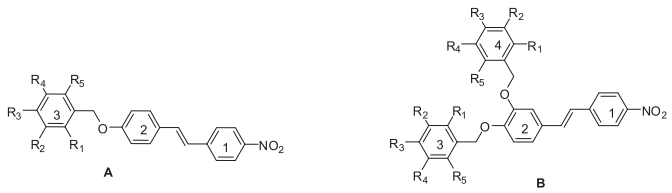

Dihedral angles between phenyl rings (°)	G1				G2			
	C1	**C2**	**C3**	**C4**	**C5**	**C6**	**C7**	**C8**
1–2	0.175	0.0926	0.0513	0.0553	0.103	0.942	1.077	1.600
2–3	39.102	43.171	49.931	71.892	40.301	44.102	52.781	75.315
2–4					−42.685	−45.156	−56.632	−73.645

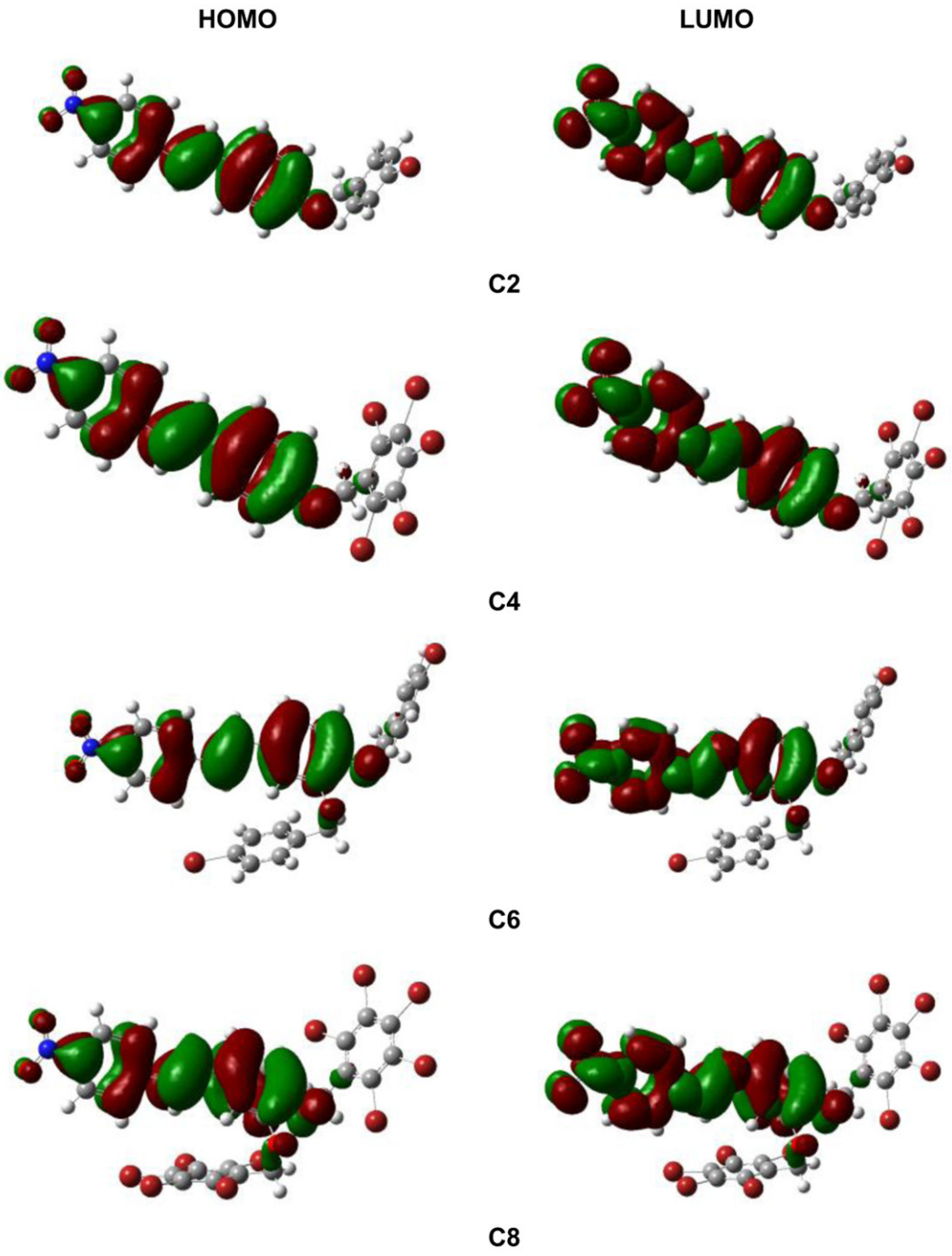

Fig. 6. The electron cloud density distributions in the frontier orbital of the photosensitizers **C2**, **C4**, **C6**, and **C8**.

C5–**C8** are accordingly red-shifted with respect to those of **C1**–**C4**. It is worth pointing out that the molecular modeling was assumed in vacuum condition, so the calculated absorption and emission maxima of the photosensitizers are smaller than those measured experimentally in the solvents.

2.4. Effects on photoluminescence yields

As our assumption, the emission intensities and the fluorescence quantum yields (Φ) of **C1**–**C4** and **C5**–**C8** are lowered by bromine atoms due to heavy atom effect (Fig. 3c and d, Table 1). It is *unexpected* that **C5**–**C8** display stronger emission and larger fluorescence quantum yields (Φ) than **C1**–**C4** in modest polar solvents such as THF and EtOAc, although they have more bromine atoms (typically shown in Fig. 4; in EtOAc, Φ: **C2**, 0.030, **C6**, 0.202; in THF, Φ: **C2**, 0.062, **C6**, 0.309). It looks *unusual* because more numbers of bromine atoms mean the larger possibility to diminish the emission of the photosensitizers due to heavy atom effect. The results indicate that heavy atom effect could be not *ONLY* one factor inherently influencing the deactivation of the excited singlet states of **C1**–**C8**.[31]

As observed in many similar diphenylethylene derivatives, twisted intramolecular charge transfer could be the other mechanism to quench the singlet states of **C1**–**C8**.[32,33] On the other hand, twisted intramolecular charge transfer could be varied by the molecular structural characteristics and the polarity of the solvents.[32] It is obvious that the molecular twist in the excited states of **C5**–**C8** could be sterically hindered by the heavy chains, although they have larger internal charge transfer ability. Hence, in low or modest polar

Table 3
Theoretically calculated dipole moment differences between the excited states and ground states of the photosensitizers

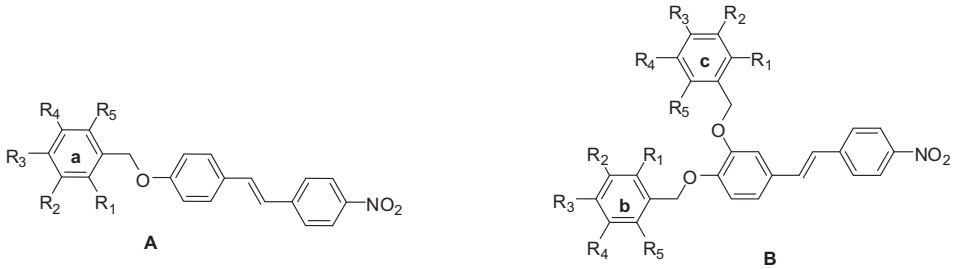

Photosensitizers		Sum of charge in phenyl ring carrying bromine atoms	Dipole moment differences ($\Delta\mu$, D)
G1	**C1**	Ring a: −0.014	1.680
	C2	Ring a: −0.029	1.424
	C3	Ring a: −0.054	1.121
	C4	Ring a: −0.109	0.533
G2	**C5**	Ring b: −0.023; ring c: −0.027	2.231
	C6	Ring b: −0.036; ring c: −0.042	1.824
	C7	Ring b: −0.059; ring c: −0.060	1.575
	C8	Ring b: −0.124; ring c: −0.085	1.082

Table 4
Theoretically calculated singlet-singlet transition energies (H−L gaps, ΔE, eV), absorption and fluorescence maxima (λ, nm) of the photosensitizers at the TDDFT//HF and TDDFT//CIS//HF level

Photosensitizers	Absorption and emission	H−L gaps (E, eV)	λ(nm)
C1	A	3.42	362.8
	E	3.07	404.2
C2	A	3.52	352.4
	E	3.11	398.9
C3	A	3.55	349.4
	E	3.14	395.2
C4	A	3.62	343.1
	E	3.20	387.8
C5	A	3.26	380.1
	E	2.92	424.2
C6	A	3.34	370.7
	E	2.96	419.5
C7	A	3.41	364.0
	E	2.97	418.0
C8	A	3.46	358.7
	E	3.00	413.3

solvents such as THF, it could not be easy to form twisted intramolecular charge transfer state for **C5**–**C8**. Normally, the solute–solute intermolecular collision possibility could be limited by its large size, which could lead to diminish photoinduced solute–solute intermolecular interaction (energy and electron transfer).[34] The above two factors could explain that the emission of **C5**–**C8** is stronger than that of **C1**–**C4** in THF (typically shown in Fig. 7).

Fig. 7. Photoluminescence of **C2** and **C6** in the solvents excited by 365 nm. From left to right: **C2**, **C6** in THF; **C2**, **C6** in acetonitrile.

In contrast, **C1**–**C4** display accordingly much stronger emission and higher fluorescence quantum yields than **C5**–**C8** in strong polar solvents, such as acetonitrile (Table 4). It is well-accepted that the strong polar solvents are much more favorable for internal charge transfer for a molecule.[32] This means that even if the molecular twist in the excited states of **C5**–**C8** could be prohibited by the heavy chains, they still could have larger possibility to undergo twisted intramolecular charge transfer in very strong polar solvents such as acetonitrile due to containing more oxygen donors.[32,33] As a consequence, the fluorescence emissions of **C1**–**C4** are correspondingly stronger than **C5**–**C8** in acetonitrile (typically shown in Fig. 7).

2.5. Effects on two-photon optical properties

Femtosecond near-IR Ti:squassier laser tuning from 700 nm to 880 nm at 20 nm step was used to determine two-photon optical properties of **C1**–**C8**. Fig. 8 presents representative TPA fluorescence emission spectra of the photosensitizers in THF excited by 760 nm femtosecond laser. As given in Fig. 8, two-photon emission intensities of **C1**–**C8** are reduced by the bromine atoms. TPA cross-sections of **C1**–**C8** were determined according to TPA fluorescence emission method. Fig. 9 shows that TPA cross-sections of **C1**–**C8** are diminished by bromine atoms under various near-IR femtosecond laser frequencies (such as **C1**, 56 GM **C2**, 37 GM, **C3**, 26 GM, **C4**, 20 GM under 760 nm laser excitation). As discussed above, the extent of intramolecular charge transfer of **C1**–**C4** and **C5**–**C8** could be lowered by the substituted bromine atoms. This means that the transition dipole moment changes between the excited and ground states of **C1**–**C4** and **C5**–**C8** could be diminished by bromine substitution accordingly. On the other hand, the coplanarity of **C1**–**C8** could be decreased by bromine atoms. These could cause the diminishments of TPA cross-sections of **C1**–**C4** and **C5**–**C8** by bromine atoms.[35]

We would point out that **C5**–**C8** show much stronger TPA unconverted fluorescence emission with longer wavelengths and larger TPA cross-sections than **C1**–**C4** (typically shown in Fig. 10, TPA, **C2**, 37 GM, **C6**, 153 GM in THF under 760 nm laser excitation), although **C5**–**C8** contain more bromine atoms. These phenomena demonstrate that side-chained structure could increase TPA cross-sections of the molecules. The results could be ascribed to more extent of internal charge transfer due to containing more oxygen

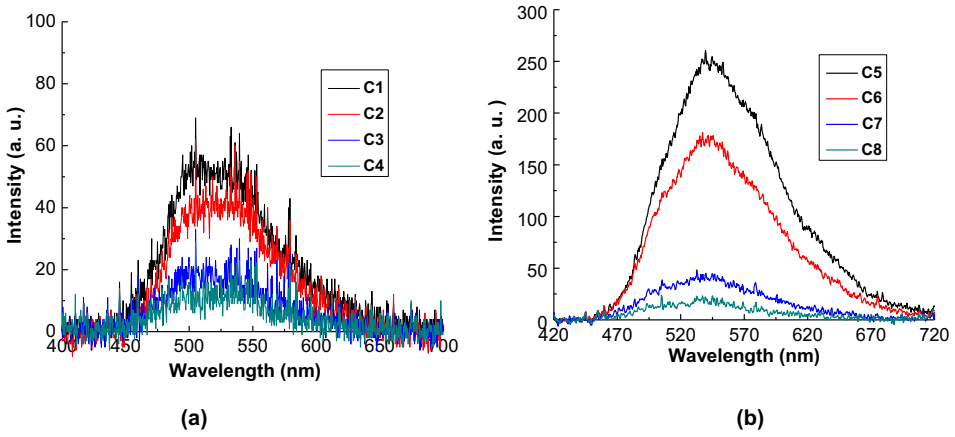

Fig. 8. TPA fluorescence emission of **C1**–**C8** excited by 760 nm femtosecond laser in THF, *c*: 1×10^{-4} mol/L.

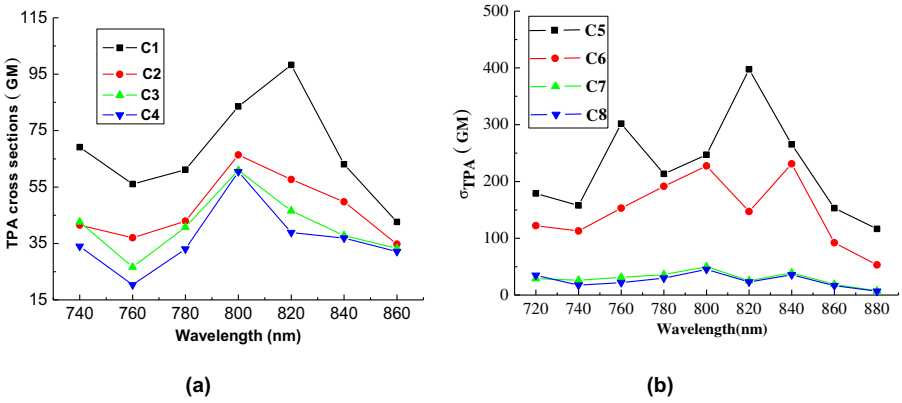

Fig. 9. TPA cross-sections of **C1**–**C8** under femtosecond laser wavelengths from 700 to 880 nm in THF.

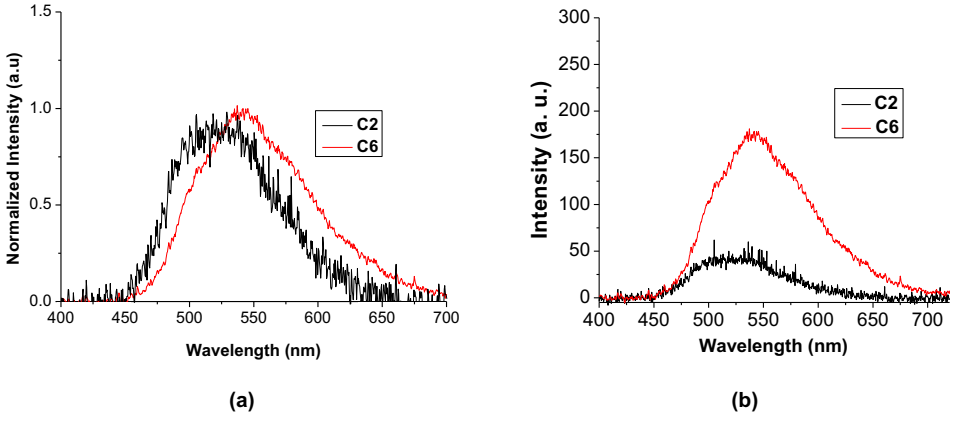

Fig. 10. Typical comparisons of two-photon emission spectra of **C2** and **C6** in THF, performed at the same experimental condition, under 760 nm, *c*: 1×10^{-4} mol/L. (a): Normalized TPA emission spectra of **C2**, **C6**; (b): real TPA emission spectra of **C2**, **C6**.

donors and more extended structure in the three-dimensional space for **C5**–**C8**.[36] It could also interpret that one- and two-photon emission maxima of **C5**–**C8** are correspondingly shifted bathochromically with respect to those of **C1**–**C4**. TPA emission maxima of **C1**–**C8** under various near-IR femtosecond laser wavelengths are irrespective of excited near-IR laser wavelengths, and they are similar to the maximal one-photon emission wavelengths (e.g., the maximal emission wavelength of **C6** in THF, one-photon is 526 nm, two-photon under 760 nm laser excitation is 536 nm).

In a word, the experimental and molecular modeling give powerful evidences that the absorption and emission maxima (one- and two-photon) of **C1**–**C8** are blue-shifted by bromine atoms. And, it is reasonable that TPA cross-sections of **C1**–**C8** are diminished by bromine atoms as well. The calculation could explain that **C5**–**C8** possess correspondingly longer absorption and emission maxima (one- and two-photon) and larger TPA cross-sections as comparison with **C1**–**C4**.

2.6. Effects on photosensitized generation of singlet oxygen

As electron-rich substrate, 2,3-dihydropyran could react with singlet oxygen to yield characteristic photooxidation products,

which in turn could determine the photosensitized generation of singlet oxygen. Under the filtered tungsten–iodine lamp or femtosecond near-IR laser irradiation, oxygen gas was kept bubbling into the quartz cell containing the solutions of singlet oxygen photosensitizer and 2,3-dihydropyran. It is assumed that the triplet states of the photosensitizers could be produced via intersystem crossing (ISC) from the singlet states, and then singlet oxygen is produced by the energy transfer from the triple states of the photosensitizers to the ground state of molecular oxygen (Scheme 2a). Representative $^1O_2$-photooxidation products detected by GC–MS confirm photosensitized generation of singlet oxygen by **C1**–**C8** under one- and two-photon irradiation (shown in Scheme 2b). The ratio of the photooxidation products 4-formoxybutanal to dihydropyrone was dependent on the solvent polarity.[37] Non-polar solvents were favorable for the production of 4-formoxybutanal via ene reaction, while dihydropyrone was mainly yielded in polar solvents. Representative triplet ESR peaks of nitro-oxide radial of 2,2,6,6-tetramethylpiperidine-1-oxyl (TEMPO),[38] which was produced from $^1O_2$-photooxidation of TEMP, demonstrate further singlet oxygen generation by **C1**–**C8** (see Supplementary data). No superoxide could be determined from the photooxidation products and ESR experiments. While enough efficient singlet oxygen quencher such as 1,4-diazobicyclo[2.2.2]octane (DBACO) was added into the above organic photochemical systems, $^1O_2$-photooxidation products or ESR signal of TEMPO could not be obtained. These results suggest that singlet oxygen could be produced by the energy transfer between the triplet state of the photosensitizers and the ground state oxygen irradiated by regular lamp (one-photon process) and near-IR femtosecond laser (two-photon process).

Table 5
Singlet oxygen quantum yields of the photosensitizers in various solvents

Photosensitizers		Singlet oxygen quantum yields			
		Benzene	EtOAc	THF	CH_3CN
G1	**C1**	0.261	0.323	0.354	0.634
	C2	0.293	0.367	0.395	0.635
	C3	0.308	0.416	0.433	0.656
	C4	0.369	0.453	0.492	0.715
G2	**C5**	0.334	0.413	0.432	0.715
	C6	0.387	0.462	0.493	0.731
	C7	0.401	0.535	0.576	0.768
	C8	0.422	0.571	0.591	0.871

from the triple states of the photosensitizers and the ground state of molecular oxygen. For instance, the quantum yield of singlet oxygen of **C1** was measured as 0.354 in THF, while the quantum yield of singlet oxygen of **C4** was improved roughly 1.4 times (0.492, in THF). **C5**–**C8** have higher singlet oxygen quantum yields than **C1**–**C4** (ca. 1.2–1.3 times) in various solvents. Although single oxygen quantum yields of **C1**–**C8** could be improved at some extents by bromine atoms, respectively, TPA cross-sections are decreased more remarkably by more bromine substitution (see Fig. 9). However, singlet oxygen quantum yields and TPA cross-sections of **C5**–**C8** could be improved simultaneously by side-chained structure. Singlet oxygen quantum yields could be enhanced in polar solvents. It could be supposed that the polarity could be favorable for the formation of $(\pi,\pi^*)^1$ of these photosensitizers since the excited states are characterized with internal charge nature, thus $(\pi,\pi^*)^3$ could be easily formed in polar solvents accordingly.

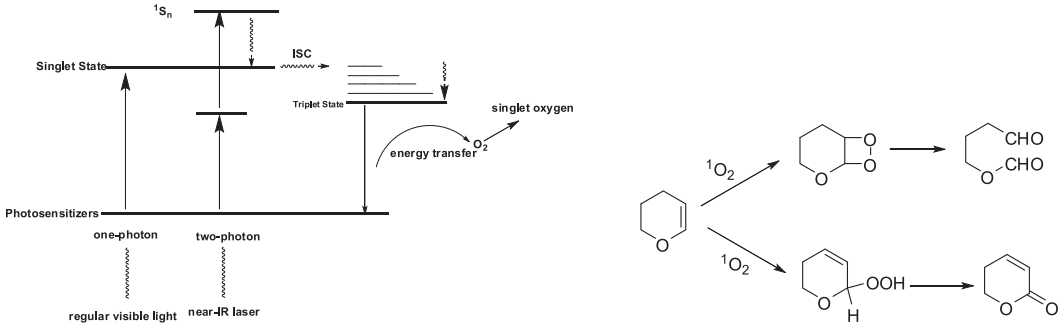

Scheme 2. Singlet oxygen generation under one- and two-photon process and photooxidation of 2,3-dihydropyran.

Singlet oxygen quantum yield reflects quantitatively the efficiency of singlet oxygen generated by the excited-state photosensitizer. One-photon singlet oxygen quantum yields of these photosensitizers were determined by the photobleaching method of 9,10-diphenylanthracene (DPA) (see Supplementary data). It could be deduced from Kasha's rule that the yield of singlet oxygen is irrelevant to the method by which initial excitation is achieved.[19] Hence, the quantum yield of singlet oxygen generated by two-photon excitation is assumed to be identical to that produced from one-photon excitation.[19] Although there are some controversies,[39] it is accepted widely that two-photon singlet oxygen quantum yields are shown positive interrelationship with one-photon singlet oxygen quantum yields.

Table 5 shows that singlet oxygen quantum yields of the photosensitizers are enhanced gradually by the substitution of bromine atoms, which reflects that heavy atom effect would be favorable for the yield of the excited triplet states of photosensitizers. This also indicates that singlet oxygen is produced by the energy transfer

3. Conclusions

To be summarized, this article reports a variety of linear and side-chained TPA singlet oxygen photosensitizers containing bromine atoms. Singlet crystal analysis suggests that the molecular coplanarity of the photosensitizers is reduced by the substitution of bromine atoms. One- and two-photon absorption and emission properties have shown the dependence on the numbers of bromine atoms. The side-chained photosensitizers exhibit much stronger photoluminescence in modest polar solvents, although they contain more bromine atoms than the linear photosensitizers. Singlet oxygen quantum yields of the photosensitizers are improved at certain extents by the bromine atoms, but TPA cross-sections are reduced remarkably. On the other hand, singlet oxygen quantum yields and TPA cross-sections of the photosensitizers could be improved by the side-chained construction. Construction of dendric or hyperbranched derivatives with a few numbers of bromine atoms as potential singlet oxygen photosensitizers could be efficient chemical

approach to realize TPA PDT. This study presents strong evidences that the numbers of bromine atoms could be optimized to obtain ideal TPA photosensitizers for the generation of singlet oxygen. In conclusion, the result shown herein would benefit to develop new TPA singlet oxygen photosensitizers, and for near-IR TPA PDT eventually. Singlet oxygen generation by these photosensitizers under femtosecond near-IR laser was confirmed by chemical approach.

4. Experimental section

4.1. Materials and characterization

Organic solvents obtained from Chongqing Medical and Chemical Corporation were further purified by standard methods.[40] The other chemicals and reagents were purchased from Aldrich unless otherwise specified. All photosensitizers, 4-nitro-4′-(phenyl-methyl-oxy)-diphenylethylene (**C1**), 4-nitro-4′-(4″-bromo-phenyl-methyl-oxy)-diphenylethylene(**C2**), 4-nitro-4′-(3″,5″-dibromo-phenyl-methyl-oxy)-diphenylethylene (**C3**), 4-nitro-4′-(2′,3″, 4′,5″,6″-pentabromo-phenyl-methyl-oxy)-diphenylethylene (**C4**), 4-nitro-3′,4′-bis(phenyl-methyl-oxy)-diphenylethylene (**C5**), 4-nitro-3′,4′-bis(4″-bromo-phenyl-methyl-oxy)-stilbene (**C6**), 4-nitro-3′,4′-bis(3″,5″-dibromo-phenyl-methyl-oxy)-diphenylethylene (**C7**), and 4-nitro-3′,4′-bis(2″,3″,4″,5″, 6′-pentabromo-phenyl-methyl-oxy)-diphenylethylene (**C8**) were synthesized in our laboratory, which were presented in Scheme 3. The photosensitizers containing bromine atoms were reported firstly in this work.

$$\Phi_f = \Phi_f^0 \frac{n_0^2 A^0 \int I_f(\lambda_f)\,d\lambda_f}{n^2 A \int I_f^0(\lambda_f)\,d\lambda_f} \quad (1)$$

in which n_0 and n represent the refractive indices of the solvents, A^0 and A denote the optical densities at excitation wavelength, Φ_f and Φ_f^0 are the quantum yields, and the integrals mean the area of the fluorescence bands for the reference and sample, respectively.

4.3. Two-photon spectral determination

Two-photon excited fluorescence spectra, pumped by Ti:sapphire femtosecond 700–880 nm laser of Spectra-Physics Ltd (Tsunami mode—locked, 80 MHz, <130 fs, average power ≤700 mW) tuned at 20 nm step, were registered on Ocean Optics USB2000 CCD camera. Up-conversion fluorescence method was utilized to determine TPA cross-section (σ) using 5×10^{-4} mol/L fluorescein in 0.1 mol/L solution of NaOH as reference.[43] The sample was bubbled with nitrogen for 15 min to eliminate oxygen before the detection. TPA cross-sections of the photosensitizers were determined by the following equations:[44]

$$\sigma = \frac{\sigma^{TPE}}{\Phi_F} \quad (2)$$

$$\sigma^{TPE} = \sigma_{cal}^{TPE} \frac{c_{cal}}{c} \frac{n_{cal}}{n} \frac{S}{S_{cal}} \quad (3)$$

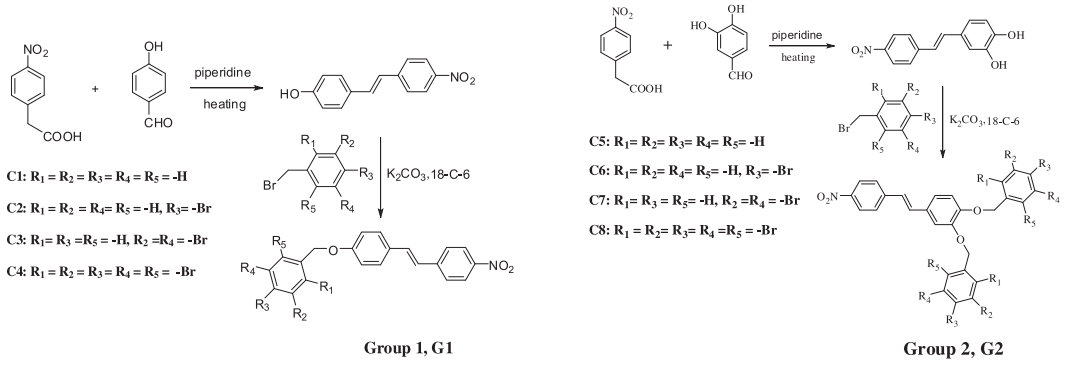

Scheme 3. Synthesis routes of the photosensitizers in this study.

Nuclear magnetic resonance (NMR) spectra were performed at the room temperature on a Bruker 500 MHz apparatus using tetramethylsilane (TMS) as an internal standard. Elemental analysis was determined with a CE440 elemental analysis meter from Exeter Analytical Inc. Beijing Fukai melting point apparatus was utilized to measure the melting points of the photosensitizers.

4.2. One-photon spectral determination

Cintra spectrophotometer was employed to measure ultraviolet/visible absorption spectra (1×10^{-5} mol/L). Shimadzu RF-531PC spectrofluorophotonmeter was utilized to detect emission spectra (1×10^{-5} mol/L). Fluorescence quantum yields (Φ) of the photosensitizers herein were detected with rodamin 6G in ethanol (Φ, 0.94, 1×10^{-6} to 1×10^{-5} mol/L) or quinoline sulfate in 0.1 mol/L H_2SO_4 (Φ, 0.55) as the references.[41] The optical density of the photosensitizers at the excited wavelength was lower than 0.1 to reduce errors of the fluorescence quantum yields. According to references,[42] the fluorescence quantum yields of a compound in various solvents with different polarities were determined based on the following equation:

where σ denotes two-photon absorption section, σ^{TPE} represents two-photon excited crossing section, c is concentration of reference and sample molecules, n is refractive index of the solvent, and S denotes two-photon up-conversion fluorescence intensity, cal represents reference.

We also detected two-photon fluorescence spectra excited by various pumped powers of near-IR laser in order to remove saturation photophysical processes and ensure two-photon excited fluorescence intensity being quadratically dependent on excitation intensity, the excitation powers in TPA cross-section measurements were limited below 130 mW.

4.4. Molecular modeling

Gaussian 03 program package was utilized for the molecular geometry optimization. All calculations were performed with 6-31G** basis set. The geometry optimization in the ground states of the photosensitizers was performed with HF method and at DFT level using B3LYP method both,[45–48] while the combination of HF and CIS was employed to optimize the geometries of the first singlet excited state (S_1) of the photosensitizers. Although CIS method

could provide reliable geometries and force-fields, it is supposed to produce too high excitation energies (ca. 1 eV).[45] To correct the errors and introduce the dynamic electron correlation, DFT and TDDFT (time-dependence DFT) were performed to predict energies at HF and CIS optimized geometries for S_0 and S_1 states, respectively, such as DFT//HF or TDDFT//CIS (denoted as single-point calculation//optimization method).[48] Herein, TDDFT//CIS was performed to analyze the emission spectra, and TDDFT//HF was used to calculate the absorption spectra.

4.4.1. Photosensitized generation of single oxygen in one- and two-photon irradiation. Oxygen-saturated solution containing the photosensitizers and the substrates in quartz cells was irradiated by the filtered tungsten–iodine lamp and near-IR laser, respectively. Photooxidation reaction of $^1O_2$ was kept at the room temperature via condenser water and strong fan to remove thermo-reaction, and UV light was endured to be blocked. After the irradiation, the oxygen-saturated solution was checked immediately by GC–MS. The products were identified using known samples and literature mass spectral data and retention times.

4.5. Preparation of single crystals and X-ray crystallography

Successfully growing of single crystals of the title compounds was carried out with slow volatilization of the solvent of their benzene solution at room temperature.

X-ray single crystal diffraction was employed to measure the crystal structures of the title compounds. XRD data were registered by a Bruker-AXS CCD area detector equipped with diffractometer with Mo Kα (λ=0.71073 Å) at 298 K. A suitable single crystal was mounted inside a glass fiber capillary. The structure of the title compound was analyzed by direct methods and refined by full-matrix least squares on F^2. All the hydrogen atoms were added in their calculated positions and all the non-hydrogen atoms were refined with anisotropic temperature factors. SHELXS97 was used to disclosure the structure, and SHELTL was used to refine the structure.[49,50]

4.6. Determination of quantum yields of singlet oxygen

Singlet oxygen quantum yields of these sensitizers were determined with the photobleaching method of 9,10-diphenylanthracence. 9,10-Diphenylanthracene (DPA) could effectively react with $^1O_2$, and an obvious photobleaching occurred. This could be observed spectrometrically for the decreasing in the 374 nm absorption peak of DPA.[51] The reaction efficiency can be expressed as following:

$$\Phi_{AO_2} = \frac{\Phi_{^1O_2}}{(\beta + [A])} \quad (4)$$

wherein Φ_{AO_2} and $\Phi_{^1O_2}$ are the quantum yields of DPA photooxygenation and single oxygen formation by the sensitizer, respectively. [A] is the concentration of DPA and β is the ratio of the chemical trapping of singlet oxygen by DPA to the physical quenching of singlet oxygen by DPA. Thus, at the same experiment condition, if a reference compound was used as the standard to determine the quantum yield of singlet oxygen formation. The following equation could be derived:

$$\frac{\Phi^X_{^1O_2}}{\Phi^S_{^1O_2}} = \frac{\Delta A_X}{\Delta A_S} \quad (5)$$

wherein $\Phi^S_{^1O_2}$ and $\Phi^X_{^1O_2}$ are the quantum yields of singlet oxygen formation by the reference and sample, respectively. ΔA_S and ΔA_X are the decreasement in the absorbance at 374 nm of the photooxygenating system sensitized by the reference and by the sample, respectively. Herein, DCA was used as a reference.

4.7. Synthesis

The photosensitizers **C1**–**C8** were synthesized based on routine routes in our laboratory (Scheme 3).

General synthesis description of title compounds. Heat condensation reaction of *p*-nitro-phenylacetic acid and corresponding benzaldehyde at 140 °C using base as catalyst yielded 4-nitro-4′-hydroxy-diphenylethylene or 4-nitro-3′, 4′-dihydroxy-diphenylethylene, which was dissolved in 18-C-6/K_2CO_3/dry acetone solution containing bromine-substituted benzyl bromide. The reactant mixture was stirred at room temperature under argon for 1 day. The solution was obtained by the filtration and the solvent was evaporated under vacuum. The obtained mixture was dissolved in $CHCl_3$ and washed with water. The organic layer was dried with anhydrous sodium sulfate and then concentrated. Further purification was performed by column chromatography and then twice recrystallization with benzene to get the title compounds.

*4.7.1. Photosensitizer **C1**.* ^{1}H NMR ($CDCl_3$, 500 MHz) δ (ppm): 5.11 (s, 2H, Ar–CH_2–O), 7.01 (t, *J*=7.8 Hz, 3H, Ar–H, –CH=CH), 7.22 (d, *J*=16.5 Hz, 1H, =CHCH), 7.34 (t, *J*=7.6 Hz, 1H, Ar–H), 7.40 (t, *J*=7.5 Hz, 2H, Ar–H), 7.45 (d, *J*=7.0 Hz, 2H, Ar–H), 7.50 (d, *J*=8.5 Hz, 2H, Ar–H), 7.60 (d, *J*=8.5 Hz, 2H, Ar–H), 8.20 (d, *J*=8.5 Hz, 2H, Ar–H). ^{13}C NMR($CDCl_3$, 125 MHz) δ (ppm): 70.105, 115.278, 124.159, 126.522, 127.473, 128.119, 128.440, 128.659, 129.219, 132.864, 136.636, 144.263, 146.451, 159.441. Yellow solid, melting point: 197–198 °C, yield: 55%. Anal. Calcd for $C_{21}H_{17}NO_3$: C, 76.12; H, 5.17; N, 4.23. Found: C, 75.92; H, 5.22; N, 4.36.

*4.7.2. Photosensitizer **C2**.* ^{1}H NMR ($CDCl_3$, 500 MHz) δ (ppm): 8.195–8.212 (d, *J*=8.5 Hz, 2H, Ar–H), 7.587–7.603 (d, *J*=8.0 Hz, 2H, Ar–H), 7.483–7.531 (m, 4H, Ar–H), 7.307–7.360 (2H, Ar–H), 7.200–7.233 (d, 1H, –CH=CH–), 6.960–7.027 (m, 3H, Ar–H, –CH=CH–), 5.153 (s, 2H, Ar–CH_2–O). ^{13}C NMR (DMSO-d_6, 125 MHz) δ (ppm): 68.453, 115.201, 120.976, 124.024, 126.891, 128.622, 129.265, 129.826, 131.361, 132.922, 136.358, 144.450, 145.804, 158.655. Yellow solid, melting point: 216.4–217.5 °C, yield: 65%. Anal. Calcd for $C_{21}H_{16}BrNO_3$: C, 61.48; H, 3.93; N, 3.41. Found: C, 61.53; H, 3.84; N, 3.37.

*4.7.3. Photosensitizer **C3**.* ^{1}H NMR (DMSO-d_6, 500 MHz) δ (ppm): 8.210–8.228 (d, *J*=9.0 Hz, 2H, Ar–H), 7.812–7.829 (d, *J*=8.5 Hz, 3H, Ar–H), 7.695–7.697 (d, *J*=1.0 Hz, 2H, Ar–H), 7.635–7.652 (d, *J*=8.5 Hz, 2H, Ar–H), 7.472–7.505 (d, 1H, *J*=16.5 Hz, –CH=CH–), 7.269–7.302 (d, 1H, *J*=16.5 Hz, –CH=CH–), 7.072–7.089 (d, 2H, Ar–H), 5.180 (s, 2H, Ar–CH_2–O). ^{13}C NMR (DMSO-d_6, 125 MHz) δ (ppm): 67.463, 115.184, 122.499, 124.010, 126.896, 128.653, 129.354, 129.473, 132.724, 132.839, 141.743, 144.403, 145.813, 158.341. Yellow solid, melting point: 159.3–160.2 °C, yield: 62%. Anal. Calcd for $C_{21}H_{15}Br_2NO_3$: C, 51.56; H, 3.09; N, 2.86. Found: C, 51.63; H, 3.14; N, 2.73.

*4.7.4. Photosensitizer **C4**.* ^{1}H NMR (DMSO-d_6, 500 MHz) δ (ppm): 8.219–8.225 (d, *J*=8.0 Hz, 2H, Ar–H), 7.813–7.830 (d, *J*=8.5 Hz, 2H, Ar–H), 7.600–7.617 (d, *J*=8.5 Hz, 2H, Ar–H), 7.470–7.503 (d, 1H, *J*=8.0 Hz, –CH=CH–), 7.258–7.290 (d, 1H, *J*=16.0 Hz, –CH=CH–), 6.947–6.963 (d, *J*=8.0 Hz, 2H, Ar–H), 4.867 (s, 2H, Ar–CH_2–O). Yellow solid, melting point: 255.1–256.3 °C, yield: 72%. Anal. Calcd for $C_{21}H_{12}Br_5NO_3$: C, 34.75; H, 1.67; N, 1.93. Found: C, 34.83; H, 1.74; N, 1.84.

*4.7.5. Photosensitizer **C5**.* ^{1}H NMR ($CDCl_3$, 500 MHz) δ (ppm): 8.19 (d, *J*=9.0 Hz, 2H, Ar–H), 7.57 (d, *J*=9.0 Hz, 2H, Ar–H), 7.48 (d, *J*=7.5 Hz, 4H, Ar–H), 7.39 (d, *J*=7.5 Hz, Ar–H), 7.33 (t, *J*=2.8 Hz, 2H,

Ar–H), 7.15 (d, *J*=17.5 Hz, 2H, Ar–H), 7.08 (d, *J*=9.5 Hz, 1H, CH=CH–Ar), 6.95 (d, *J*=6.5 Hz, 2H, Ar–CH=CH, Ar–H), 5.22 (s, 4H, O–CH_2–Ar). ^{13}C NMR ($CDCl_3$, 125 MHz) δ (ppm): 71.119, 113.216, 114.718, 121.394, 124.128, 126.594, 127.234, 127.352, 127.954, 128.558, 129.856, 136.922, 144.083, 146.468, 149.135, 149.915. Yellow solid, melting point: 136.5–137 °C, yield: 46%. Anal. Calcd for $C_{28}H_{23}NO_4$: C, 76.87; H, 5.30; N, 3.20. Found: C, 76.75; H, 5.39; N, 3.29.

4.7.6. Photosensitizer ***C6***. ^{1}H NMR ($CDCl_3$, 500 MHz) δ (ppm): 8.193–8.211 (d, *J*=9.0 Hz, 2H, Ar–H), 7.574–7.591 (d, *J*=8.5 Hz, 2H, Ar–H), 7.493–7.523 (t, *J*=7.5 Hz, 4H, Ar–H), 7.341–7.295 (m, 4H, Ar–H), 7.163–7.083 (m, 3H, Ar–H, –CH=CH–), 6.960–6.9079 (m, 2H, Ar–H, –CH=CH–), 5.130–5.109 (d, *J*=10.5 Hz, 4H, O–CH_2–Ar). ^{13}C NMR (DMSO-d_6, 125 MHz) δ (ppm): 150.238, 149.611, 147.090, 143.539, 136.377, 136.185, 132.708, 131.939, 129.245, 129.202, 126.631, 125.246, 124.189, 114.958, 113.738, 70.812, 70.364. Yellow solid, melting point: 159.2–161.1 °C, yield: 50%. Anal. Calcd for $C_{28}H_{21}Br_2NO_4$: C, 56.49; H, 3.56; N, 2.35. Found: C, 56.43; H, 3.45; N, 2.47.

4.7.7. Photosensitizer ***C7***. ^{1}H NMR ($CDCl_3$, 500 MHz) δ (ppm): 8.208–8.226 (d, *J*=9.0 Hz, 2H, Ar–H), 7.599–7.642 (m, 4H, Ar–H), 7.572 (s, 2H, Ar–H), 7.536 (s, 2H, Ar–H), 7.189–7.134 (m, 3H, –CH=CH–, Ar–H), 6.993–6.920 (m, 2H, Ar–H, –CH=CH–), 5.130–5.109 (d, 4H, Ar–CH_2–O). Yellow solid, melting point: 217–219 °C, yield: 40%. Anal. Calcd for $C_{28}H_{19}Br_4NO_4$: C, 44.86; H, 2.54; N, 1.86. Found; C, 44.95; H, 2.46; N, 1.97.

4.7.8. Photosensitizer ***C8***. ^{1}H NMR ($CDCl_3$, 500 MHz) δ (ppm): 8.230–8.213 (d, *J*=8.5 Hz, 2H, Ar–H), 7.612–7.630 (d, *J*=9 Hz, 2H, Ar–H), 7.363 (s, 2H, Ar–H), 7.202 (s, 1H, –CH=CH–), 7.061–7.053 (m, 2H, –CH=CH–, Ar–H), 5.507–5.501 (d, *J*=3 Hz, 4H, Ar–CH_2–O). Yellow solid, melting point: >300 °C, yield: 35%. Anal. Calcd for $C_{28}H_{13}Br_{10}NO_4$: C, 27.42; H, 1.07; N, 1.14. Found: C, 27.55; H, 1.16; N, 1.05.

Acknowledgements

We appreciate financial support from the Fundamental Research Funds for the Central Universities (CDJZR10220006). We also thank the support from Chongqing Natural Science Committees (CSTC2012jjB50007 and CSTC2010BB0216). F.G. thanks the warm encouragements from the Ministry of Education, China (NCET-10-0876). In particular, we thank the warm encouragements from National Science Foundation of China (NSFC) and Key Laboratory of Photochemical Conversion and Optoelectronic Materials, TIPC, Chinese Academy of Sciences.

Supplementary data

CCDC 821856, 885014, and 885015 contain the supplementary crystallographic date for this work. These data can be obtained free of charge via http://www.ccdc.cam.ac.uk/conts/retrieving.html or from the Cambridge Crystallographic Data Center (12, Union Road, Cambridge CB2 1EZ, UK; fax: +44 1223 336033). The crystallographic details, crystal molecular view of **C2**–**C4**, normalized absorption and emission spectra, and more molecular optimization results were included in the supplementary data. Supplementary data associated with this article can be found in the online version, at http://dx.doi.org/10.1016/j.tet.2013.02.010.

References and notes

1. DeRosa, M. C.; Crutchley, R. J. *Coord. Chem. Rev.* **2002**, *233–234*, 351.
2. (a) Tofi, M.; Koltsida, K.; Vassilikogiannakis, G. *Org. Lett.* **2009**, *11*, 313; (b) Jiang, G.; Chen, J.; Huang, J.; Che, C. *Org. Lett.* **2009**, *11*, 4568; (c) Poon, T.; Turro, N. J.; Chapman, J.; Lakshminarasimhan, P.; Lei, X.; Jockusch, S.; Franz, R.; Washington, I.; Adam, W.; Bosio, S. G. *Org. Lett.* **2003**, *5*, 4951.
3. (a) Clennan, E. L.; Pace, A. *Tetrahedron* **2005**, *61*, 6665; (b) Clennan, E. L. *Acc. Chem. Res.* **2001**, *34*, 875.
4. (a) Adam, W.; Bosio, S. G.; Turro, N. J. *J. Am. Chem. Soc.* **2002**, *124*, 8814; (b) Hecht, S.; Frechet, J. M. J. *J. Am. Chem. Soc.* **2001**, *123*, 6959.
5. Prein, M.; Adam, W. *Angew. Chem., Int. Ed.* **1998**, *35*, 477.
6. (a) Adam, W.; Bosio, S. G.; Turro, N. J.; Wolff, B. T. *J. Org. Chem.* **2004**, *69*, 1704; (b) Natarajan, A.; Kaanumalle, L. S.; Jockusch, S.; Gibb, C. L. D.; Gibb, B. C.; Turro, N. J.; Ramamurthy, V. *J. Am. Chem. Soc.* **2007**, *129*, 4132.
7. McDonnell, S. O.; Hall, M. J.; Allen, L. T.; Byrne, A.; Gallagher, W. M.; O'Shea, D. F. *J. Am. Chem. Soc.* **2005**, *127*, 16360.
8. Ozlem, S.; Akkaya, E. U. *J. Am. Chem. Soc.* **2009**, *131*, 48.
9. Clo, E.; Snyder, J. W.; Voigt, N. V.; Ogilby, P. R.; Gothelf, K. V. *J. Am. Chem. Soc.* **2006**, *128*, 4200.
10. (a) Hone, D. C.; Walker, P. I.; Evans-Gowing, R.; FitzGerald, S.; Beeby, A.; Chambrier, I.; Cook, M. J.; Russell, D. A. *Langmuir* **2002**, *18*, 2985; (b) Bakalova, R.; Ohba, H.; Zhelev, Z.; Nagase, T.; Jose, R.; Ishikawa, M.; Baba, Y. *Nano Lett.* **2004**, *4*, 1567; (c) Cheng, Y.; Samia, A. C.; Meyers, J. D.; Panagopoulos, I.; Fei, B.; Burda, C. *J. Am. Chem. Soc.* **2008**, *130*, 10643; Guo, H.; Qian, H.; Idris, N. M.; Zhang, Y. *Nanomed. Nanotechnol. Biol. Med.* **2012**, *6*, 486.
11. Gottschaldt, M.; Schubert, U. S.; Rau, S.; Yano, S.; Vos, J. G.; Kroll, T.; Clement, J.; Hilger, I. *ChemBioChem* **2010**, *11*, 649.
12. Silva, E. F. F.; Serpa, C.; Dąbrowski, J. M.; Monteiro, C. J. P.; Formosinho, S. J.; Stochel, G.; Urbanska, K.; Simoe, S.; Pereira, M. M.; Arnaut, L. G. *Chem.—Eur. J.* **2009**, *30*, 9273.
13. Pawlicki, M.; Collins, H. A.; Denning, R. G.; Anderson, H. L. *Angew. Chem., Int. Ed.* **2009**, *48*, 3244.
14. (a) Chung, S.; Zheng, S.; Odani, T.; Beverina, L.; Fu, J.; Padilha, L. A.; Biesso, A.; Hales, J. M.; Zhan, X.; Schmidt, K.; Ye, A.; Zojer, E.; Barlow, S.; Hagan, D. J.; Van Stryland, E. W.; Yi, Y.; Shuai, Z.; Pagani, G. A.; Bredas, J.; Perry, J. W.; Marder, S. R. *J. Am. Chem. Soc.* **2006**, *128*; (b) Paterson, M. J.; Kongsted, J.; Christiansen, O.; Mikkelsen, K. V.; Nielsen, C. B. *J. Chem. Phys.* **2006**, *125*, 184501.
15. Kim, S.; Ohulchanskyy, T. Y.; Pudavar, H. E.; Pandey, R. K.; Prasad, P. N. *J. Am. Chem. Soc.* **2007**, *129*, 2669.
16. (a) Drobizhev, M.; Stepanenko, Y.; Dzenis, Y.; Karotki, A.; Rebane, A.; Taylor, P. N.; Anderson, H. L. *J. Am. Chem. Soc.* **2004**, *126*, 15352; (b) Goyan, R.; Cramb, D. *Photochem. Photobiol.* **2000**, *72*, 821.
17. (a) Drobizhev, M.; Stepanenko, Y.; Dzenis, Y.; Karotki, A.; Rebane, A.; Taylor, P. N.; Anderson, H. L. J. *Phys. Chem. B* **2005**, *109*, 7223; (b) Karotki, A.; Khurana, M.; Lepock, J. R.; Wilson, B. C. *Photochem. Photobiol.* **2006**, *82*, 443.
18. Morone, M.; Beverina, L.; Abbotto, A.; Silvestri, F.; Collini, E.; Ferrante, C.; Bozio, R.; Pagani, G. A. *Org. Lett.* **2006**, *8*, 2719.
19. Frederiksen, P. K.; Jorgensen, M.; Ogilby, P. R. *J. Am. Chem. Soc.* **2001**, *123*, 1215; (a) McIlroy, S.; Clo, E.; Nikolajsen, L.; Frederiksen, P.; Nielsen, C.; Mikkelsen, K.; Gothelf, K.; Ogilby, P. R. *J. Org. Chem.* **2005**, *70*, 1134; (b) Frederiksen, P.; Mcilroy, S.; Nielsen, C.; Nikolajsen, L.; Skovsen, E.; Jorgensen, M.; Mikkelsen, K.; Ogilby, P. R. *J. Am. Chem. Soc.* **2005**, *127*, 255.
20. Dichtel, W.; Serin, J.; Edder, C.; Frechet, J. M. J.; Matuszewski, M.; Tan, L.; Ohulchanskyy, T.; Prasad, P. N. *J. Am. Chem. Soc.* **2004**, *126*, 5380.
21. Gao, D.; Agayan, R.; Xu, H.; Philbert, M.; Kopelman, R. *Nano Lett.* **2006**, *6*, 2383.
22. Bechet, D.; Couleaud, P.; Frochot, C.; Viriot, M.; Guillemin, F.; Muriel, B. *Trends Biotechnol.* **2008**, *26*, 612.
23. Shen, X.; He, F.; Wu, J.; Xu, G. Q.; Yao, S. Q.; Xu, Q. H. *Langmuir* **2011**, *27*, 1739.
24. (a) Zhang, C.; Song, Y.; Wang, X.; Kuhn, F. E.; Wang, Y.; Yan, X.; Xin, X. *J. Mater. Chem.* **2003**, *13*, 571; (b) Hou, H.; Wei, Y.; Song, Y.; Mi, L.; Tang, M.; Li, L.; Fan, Y. *Angew. Chem.* **2005**, *117*, 6221.
25. Stadler, A.-M. *Cryst. Growth Des.* **2010**, *10*, 5050.
26. (a) Kovalenko, S. A.; Schanz, R.; Farztdinov, V. M.; Hennig, H.; Ernsting, N. P. *Chem. Phys. Lett.* **2000**, *323*, 312; (b) Jenekhe, S. A.; Lu, L.; Alam, M. M. *Macromolecules* **2001**, *34*, 7315.
27. Toptygin, D. *J. Fluoresc.* **2003**, *13*, 201.
28. Cummings, S. D.; Eisenberg, R. *J. Am. Chem. Soc.* **1996**, *118*, 1949.
29. Kakkar, R.; Katoch, V. *J. Mol. Struct. (Theochem)* **2002**, *578*, 169.
30. (a) Tatchen, J.; Marian, C. M. *Phys. Chem. Chem. Phys.* **2006**, *8*, 2133; (b) Salzmann, S.; Kleinschmidt, M.; Tatchen, J.; Weinkauf, R.; Marian, C. M. *Phys. Chem. Chem. Phys.* **2008**, *10*, 380.
31. Schmidt, R. *J. Am. Chem. Soc.* **1989**, *111*, 6983.
32. (a) Letard, J. F.; Lapouyade, R.; Rettig, W. *J. Am. Chem. Soc.* **1993**, *115*, 2441; (b) Yang, J.; Liau, K.-L.; Wang, C.-M.; Hwang, C.-H. *J. Am. Chem. Soc.* **2004**, *126*, 12325.
33. (a) Eckert, C.; Heisel, F.; Miehe, J. A.; Lapouyade, R.; Ducasse, L. *Chem. Phys. Lett.* **1988**, *153*, 357; (b) Sato, Y.; Morimoto, M.; Segawa, H.; Shimidzu, T. *J. Phys. Chem.* **1995**, *99*, 35.
34. Backer, C. A.; Whitten, D. G. *J. Phys. Chem.* **1987**, *91*, 865.
35. (a) Chung, S.-J.; Kim, K.-S.; Lin, T.-C.; He, G.-S.; Swiatkiewicz, J.; Prasad, P. N. *J. Phys. Chem. B* **1999**, *103*, 10741; (b) Albota, M.; Beljonne, D.; Brédas, J.-l.; Ehrlich, J. E.; Fu, J.-Y.; Heikal, A. A.; Hess, S. E.; Kogel, T.; Levin, M. D.; Marder, S. R.; McCord-Maughon, D.; Perry, J. W.; Rokel, H.; Rumi, M.; Subramaniam, G.; Webb, W. W.; Wu, X.-L.; Xu, C. *Science* **1998**, *281*, 1653; (c) Mai, C.-L.; Liu, Y.-C.; Yeh, C.-Y.; Vura-Weis, J.; Wasielewski, M. R.; Kim, D. *J. Phys. Chem. A* **2008**, *112*, 6563; (d) Marder, S. R. *Chem. Commun.* **2006**, 131.
36. Bartholomew, G. P.; Rumi, M.; Pond, S. J. K.; Perry, J. W.; Tretiak, S.; Bazan, G. C. *J. Am. Chem. Soc.* **2004**, *126*, 11529.
37. Gao, F.; Li, H.; Li, X.; Wu, L.; Tung, C. *Colloids Surf., A: Physicochem. Eng. Asp.* **2007**, *204*, 31.

38. Li, H.; Wu, L.; Tung, C. *J. Am. Chem. Soc.* **2000**, *122*, 2446.
39. (a) Andrasik, S.; Belfield, K.; Bondar, M.; Hernandez, F.; Morales, A.; Przhonska, O.; Yao, S. *ChemPhysChem* **2007**, *8*, 399; (b) Belfield, K.; Bondar, M.; Przhonska, O. *J. Fluoresc.* **2006**, *16*, 111.
40. Perrin, D.; Armarego, W. *Purification of Laboratory Chemicals*; Pergamon: New York, NY, 1996.
41. Fischer, M.; Georges, J. *Chem. Phys. Lett.* **1996**, *260*, 115; Eaton, D. *Pure Appl. Chem.* **1998**, *60*, 1107.
42. (a) Maus, M.; Reitigg, W.; Bonafoux, D.; Lapouyade, R. *J. Phys. Chem. A.* **1999**, *103*, 3388; (b) Lukeman, M.; Veale, D.; Wan, P.; Ranjit, V.; Munasinghe, N.; Corrie, J. *Can. J. Chem.* **2004**, *82*, 240.
43. Xu, C.; Webb, W. *J. Opt. Soc. Am. B* **1996**, *13*, 481.
44. Albota, M.; Xu, C.; Webb, W. *Appl. Opt.* **1998**, *37*, 7352.
45. Zgiershi, M. Z.; Grabowska, A. *J. Chem. Phys.* **2000**, *112*, 6329.
46. Yi, P. G.; Liang, Y. H.; Cao, C. Z. *Chem. Phys.* **2005**, *315*, 297.
47. Liang, Y. H.; Yi, P. G. *Chem. Phys. Lett.* **2007**, *438*, 173.
48. Yang, Z.; Yang, S.; Zhang, J. *J. Phys. Chem. A.* **2007**, *111*, 6354.
49. Sheldrick, G. M. *SHELXS 97, Program for Crystal Structure Solution*; University of Gottingen: Gottingen, Germany, 1997.
50. Sheldrick, G. M. *SHELXL 97, Program for Crystal Structure Refinement*; University of Gottingen: Gottingen, Germany, 1997.
51. Diwu, Z.; Lownt, J. W. *J. Photochem. Photobiol., A: Chem.* **1992**, *64*, 273.